Journal of Geophysical Research – Solid Earth

Supporting Information for

Seismic array constraints on the D" discontinuity beneath Central America

Stefanie Whittaker[1], Michael S. Thorne[2], Nicholas C. Schmerr[3], and Lowell Miyagi[2]

[1]Department of Geosciences, University of Alaska Fairbanks, Fairbanks, AK, USA, [2]Department of Geology and Geophysics, University of Utah, Salt Lake City, UT, USA, [3]Department of Geology, University of Maryland, College Park, MD, USA

Contents of this file

Introduction

The supporting figures and tables provide a series of synthetic tests to show the resolution of the data, and provide a list of events used in the main article.

Figures S1 – S4 show the measurements taken from the synthetic vespagrams where a) is the differential travel time versus the D″ discontinuity height, b) is the differential travel time versus δV_S, c) is the differential slowness versus the D″ discontinuity height, d) is the differential slowness versus δV_S, e) is the amplitude ratio versus the D″ discontinuity height, and f) is the amplitude ratio versus δV_S for the bins 58°-64°, 64°-70°, 70°-76°, and 76°-82° respectively. The lines are best fit lines through the data points.

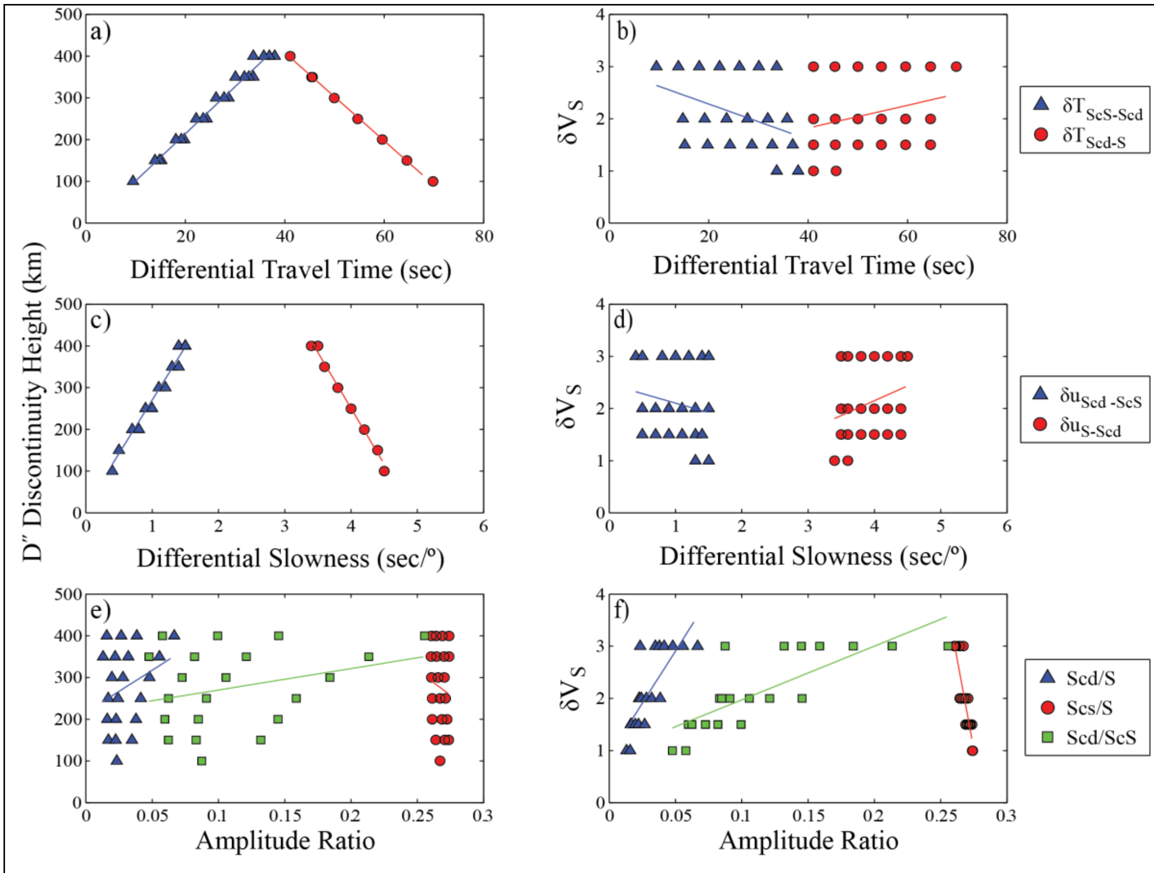

Figure S1. Epicentral distance range: 58°-64°

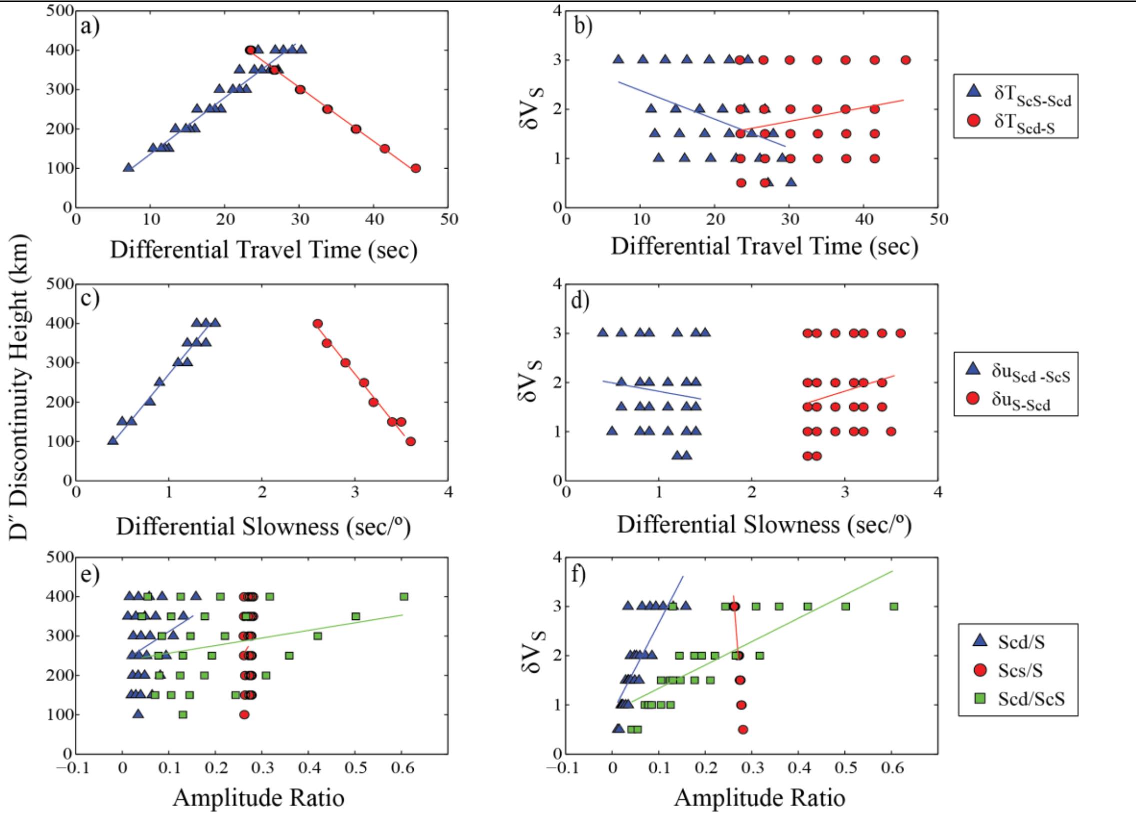

Figure S2. Epicentral distance range: 64°-70°.

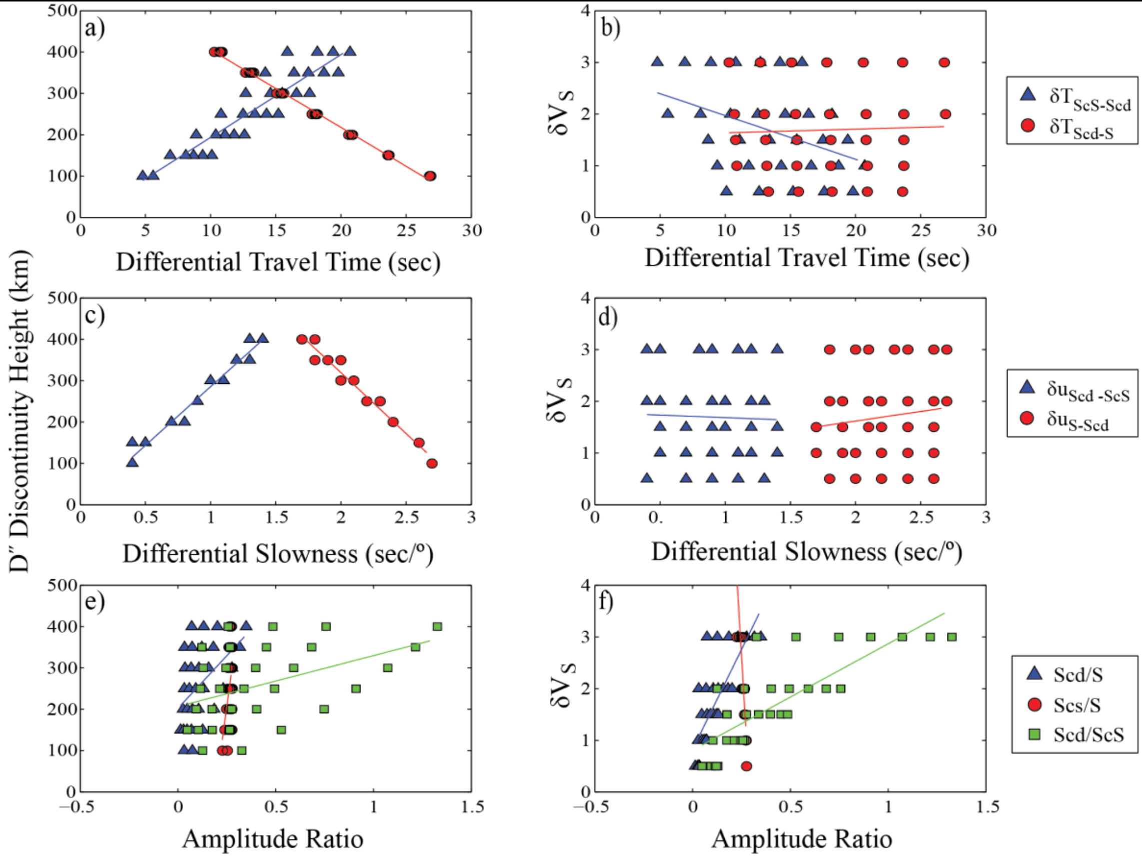

Figure S3. Epicentral distance range: 70°-76°

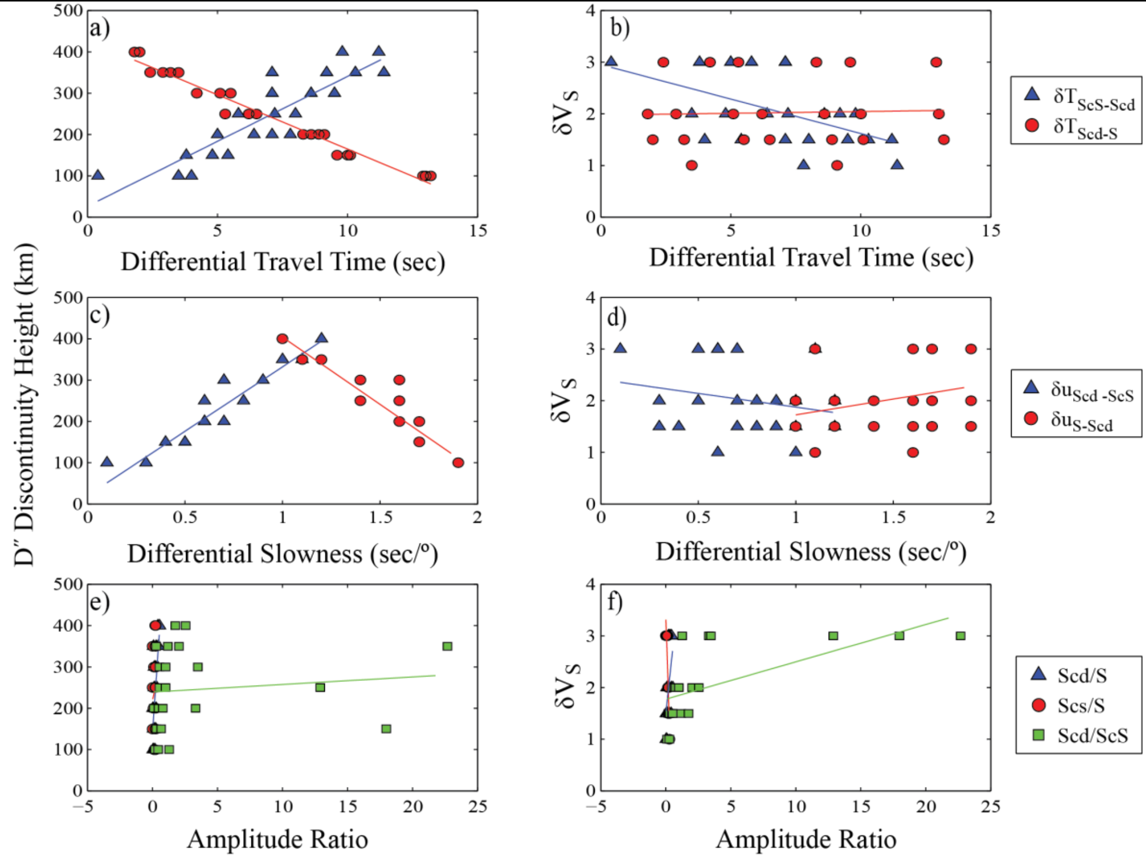

Figure S4. Epicentral distance range: 76°-82°

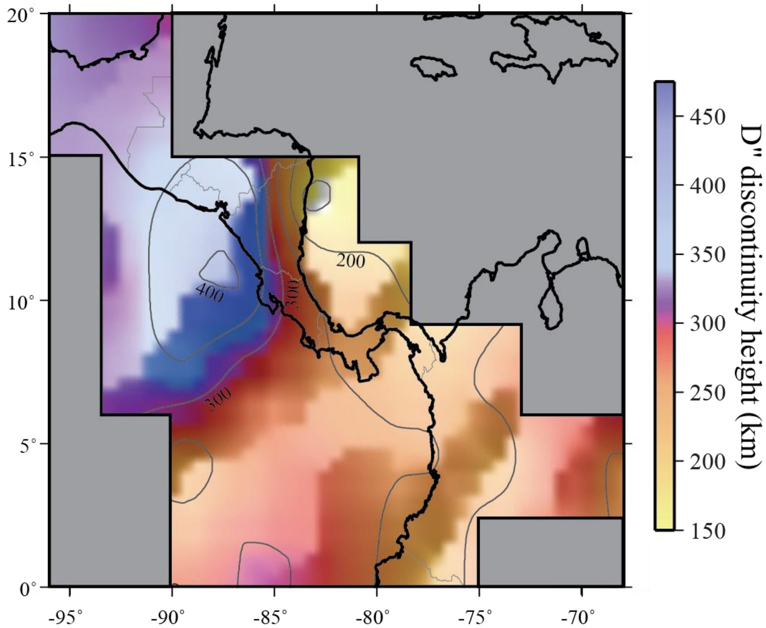

Figure S5. Contour map of the weighted average height of the D″ discontinuity using only the highest quality *Scd* picks.

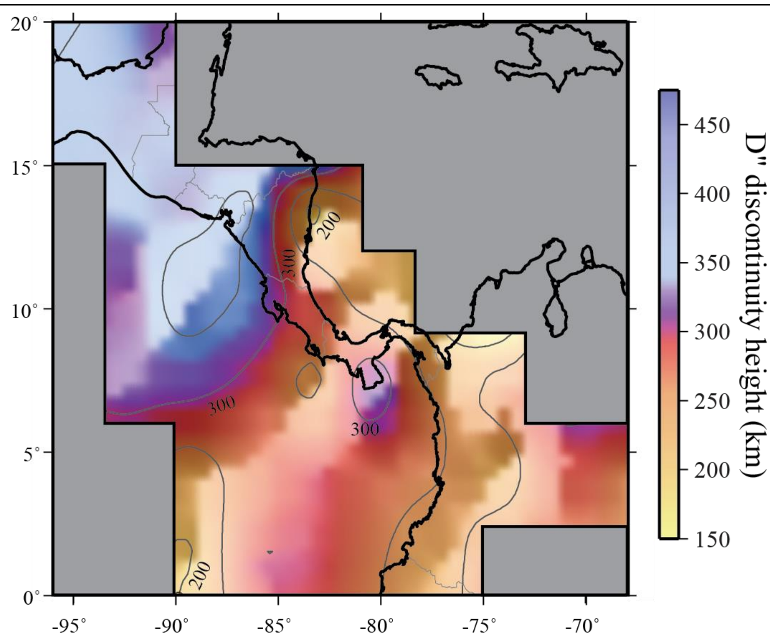

Figure S6. Contour map of the weighted average D″ discontinuity height using the low estimate of the double *Scd* arrival.

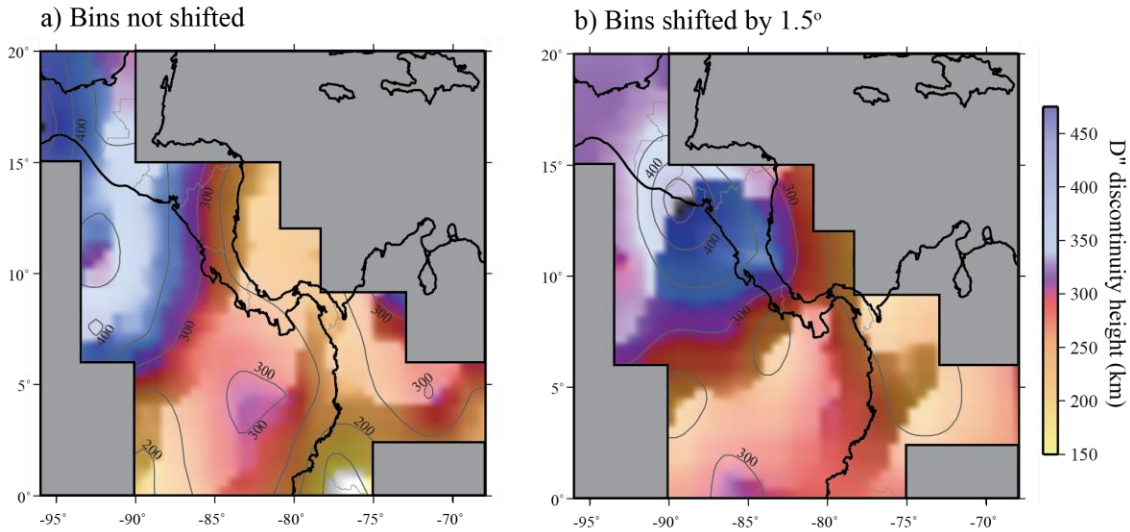

Figure S7. Contour map of the weighted average D″ discontinuity height using a) the original array bin centers, and b) shifting the bin centers in latitude and longitude by 1.5°.

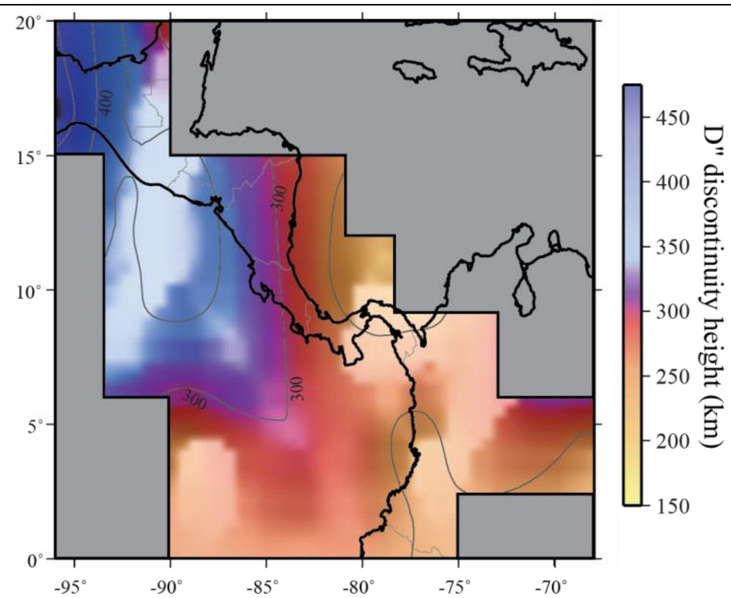

Figure S8. Contour map of the weighted average D″ discontinuity height using a minimum of 20 stations per array bin.

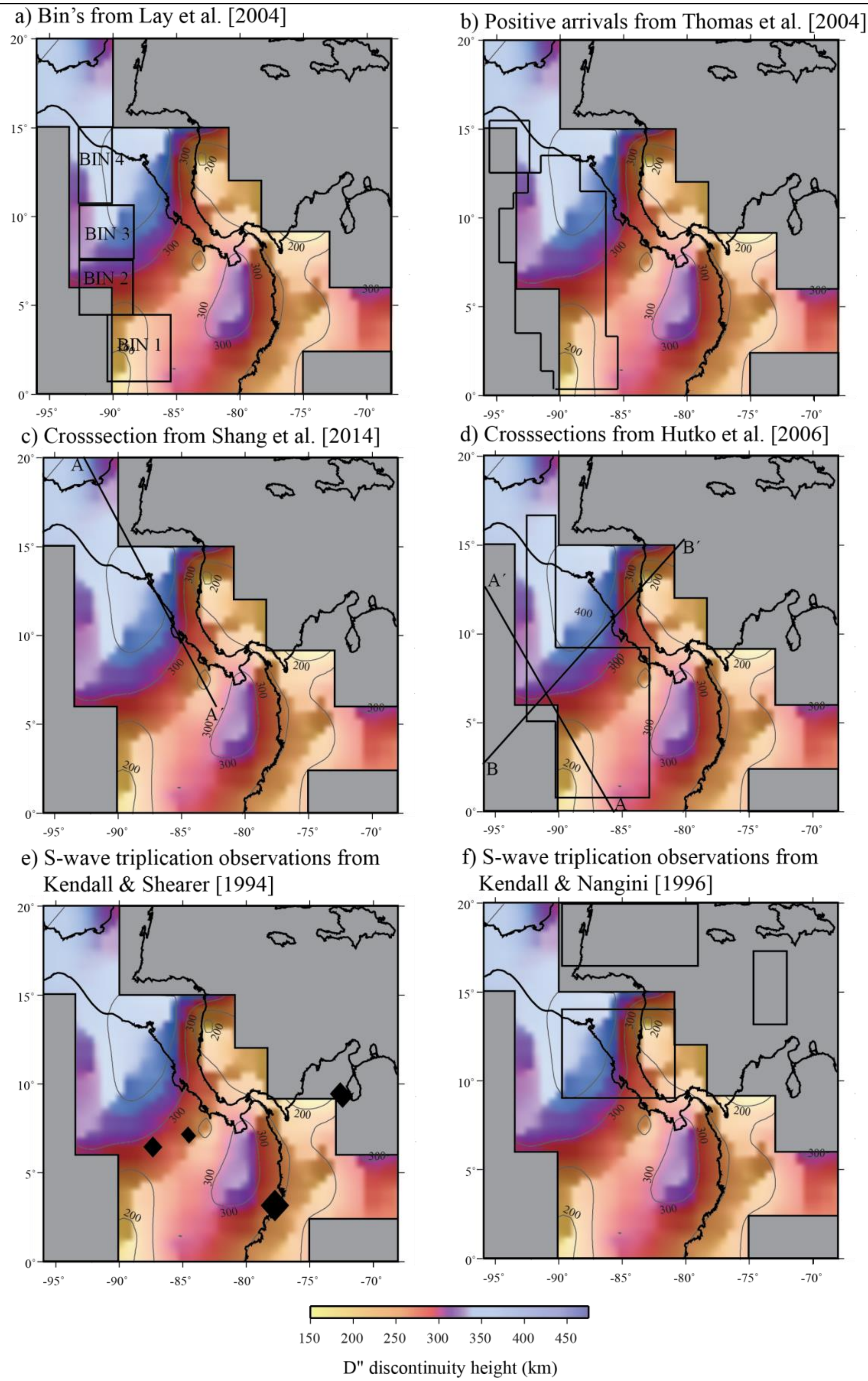
a) Bin's from Lay et al. [2004]
BIN 4
BIN 3
BIN 2
BIN 1
b) Positive arrivals from Thomas et al. [2004]
c) Crosssection from Shang et al. [2014]
d) Crosssections from Hutko et al. [2006]
e) S-wave triplication observations from Kendall & Shearer [1994]
f) S-wave triplication observations from Kendall & Nangini [1996]
150 200 250 300 350 400 450
D" discontinuity height (km)

Figure S9. Comparison of D'' discontinuity height with previous study regions. The background is our results from Fig. 6b of the main paper. a) Displays the 4 bins used in the study of *Lay et al.,* [2004]. b) The black boxes shows the area where positive arrivals were observed by *Thomas et al.,* [2004]. c) Shows the position of the *Shang et al.,* [2014] cross-section. d) Shows the positions of the cross-sections shown in the *Hutko et al.* [2006] study. e) The locations of *ScS* bouncepoints from the study of *Kendall and Shearer* [1994] are shown as black diamonds. f) The black boxes outline where the D'' discontinuity was observed in the study of *Kendall and Nangini* [1996].

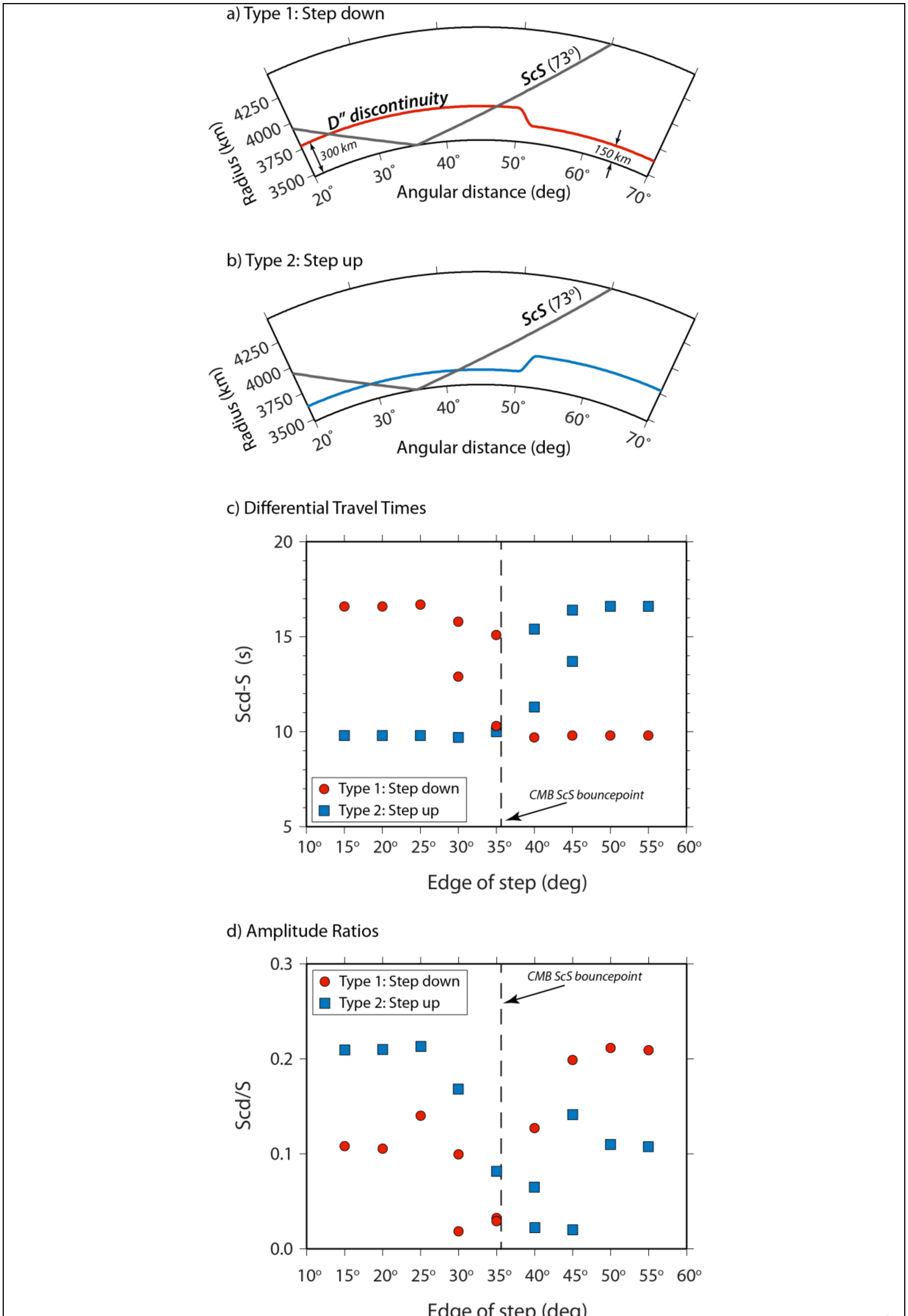
a) Type 1: Step down
ScS (73°)
D″ discontinuity
4250
4000
3750
3500
Radius (km)
300 km
150 km
20°
30°
40°
50°
60°
70°
Angular distance (deg)
b) Type 2: Step up
ScS (73°)
4250
4000
3750
3500
Radius (km)
20°
30°
40°
50°
60°
70°
Angular distance (deg)
c) Differential Travel Times
Scd-S (s)
20
15
10
5
Type 1: Step down
Type 2: Step up
CMB ScS bouncepoint
10°
15°
20°
25°
30°
35°
40°
45°
50°
55°
60°
Edge of step (deg)
d) Amplitude Ratios
Scd/S
0.3
0.2
0.1
0.0
Type 1: Step down
Type 2: Step up
CMB ScS bouncepoint
10°
15°
20°
25°
30°
35°
40°
45°
50°
55°
60°
Edge of step (deg)

Figure S10. We computed synthetic seismograms for two types of models with step-like topography as shown in panels a) and b). In both panels the source is on the left-hand side of the plot and the receiver is on the right-hand side. a) The discontinuity is drawn for a step down in topography with a red line. b) The discontinuity is drawn for a step up in topography with a blue line. The ray path for an *ScS* arrival at a distance of 73° is drawn with the gray line. In both panels a) and b) the step occurs at an angular distance of 50°. In both types of models the D" discontinuity has a height of 150 and 300 km for the two regions (shallowest height or greatest height above the CMB) and the synthetics are computed for a model with an *S*-wave velocity increase of 2% relative to PREM. c) Differential travel-times for *Scd*-*S* are shown for an array centered at 73° in epicentral distance as a function of the position of the step in discontinuity height. The results for models with a step down in topography are shown by the red circles, and the results for models with a step up in topography are shown by the blue squares. For the step down models, two *Scd* arrivals are observed when the edge of the step in the discontinuity lies between 30° and 35°. For the step up models, two *Scd* arrivals are observed when the edge of the step in the discontinuity lies between 40° and 45°. The position of the theoretical *ScS* bouncepoint for a 73° *ScS* arrival is indicated by the dashed line. d) *Scd*/*S* amplitude ratios are shown.

As an example, consider the step down model in panel a). The edge of the step is located at an angular distance of 50°. Here and *ScS* arrival at 73° encounters the portion of the discontinuity with the maximum height above the CMB. Consequently, *Scd* will arrive at its closest time with respect to the direct *S*-wave arrival. Thus the differential time *Scd*-*S* will be at a minimum when the positon of the step is at 50°. This is reflected in panel c).

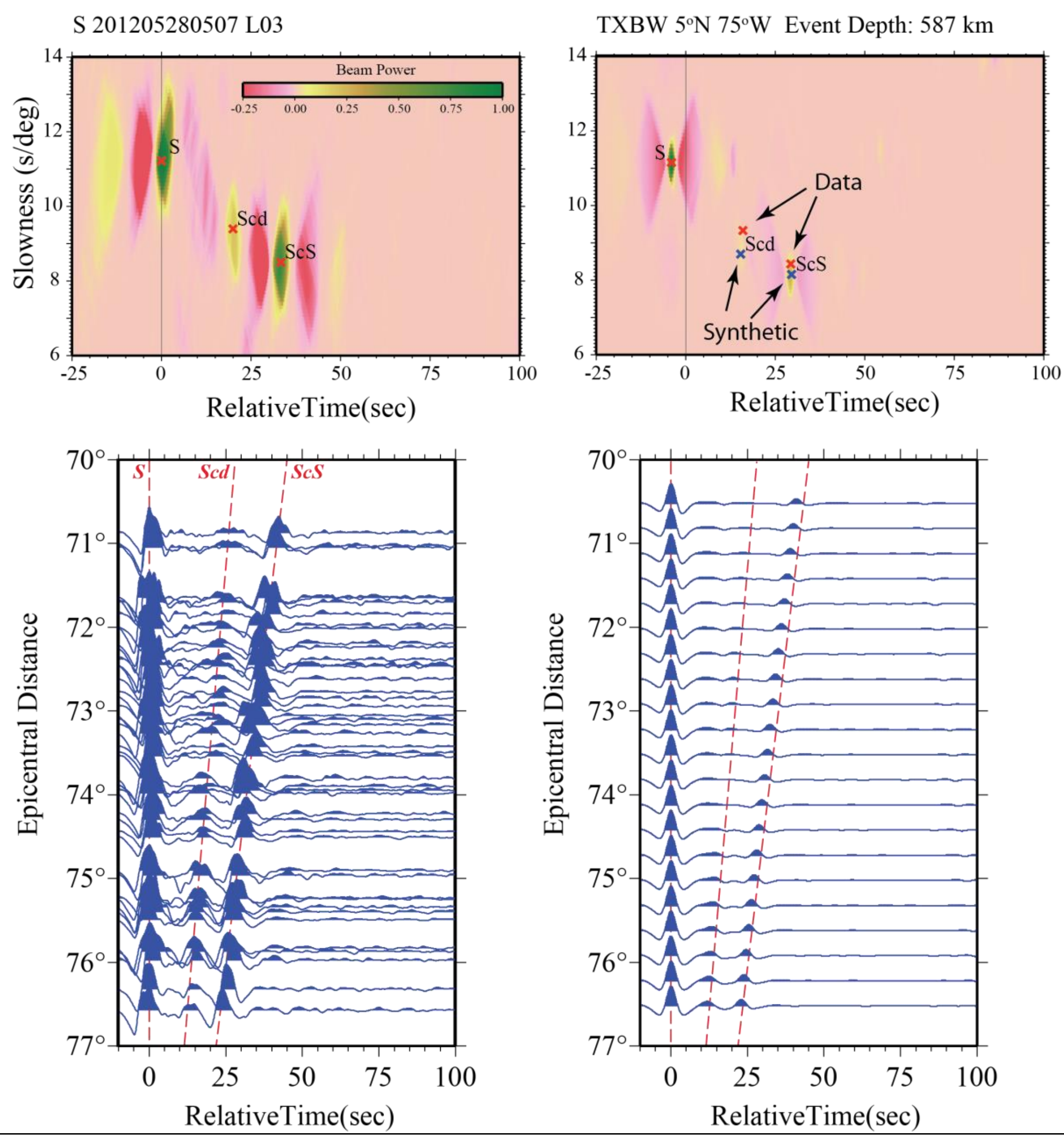

Figure S11. Vespagrams and record sections are shown for data (left hand side) and synthetic seismograms through *S*-wave velocity model TXBW [*Grand*, 2002] (right hand side). Data and synthetics are both for an event depth of 587 km, and sample a central *ScS* bounce point at 5° N, 75° W. The peaks in the vespagrams for data are drawn with red crosses and the peaks in the synthetic vespagrams are drawn with blue crosses. The red crosses for data are repeated in the synthetic vespagram for direct comparison. Note that absolute time and slowness of data peaks are shifted to be aligned with the direct S-wave arrival in the synthetic vespagram. All traces are displacement transverse component seismograms aligned and normalized to unity on the direct *S*-wave arrival. Approximate arrival times for the *Scd* and *ScS* arrivals for data are indicated by the dashed red lines and repeated in the right-hand column for comparison with synthetic predictions. Synthetic seismograms are shown for a dominant period of 10 s to match the dominant period of data shown in the left-hand column.

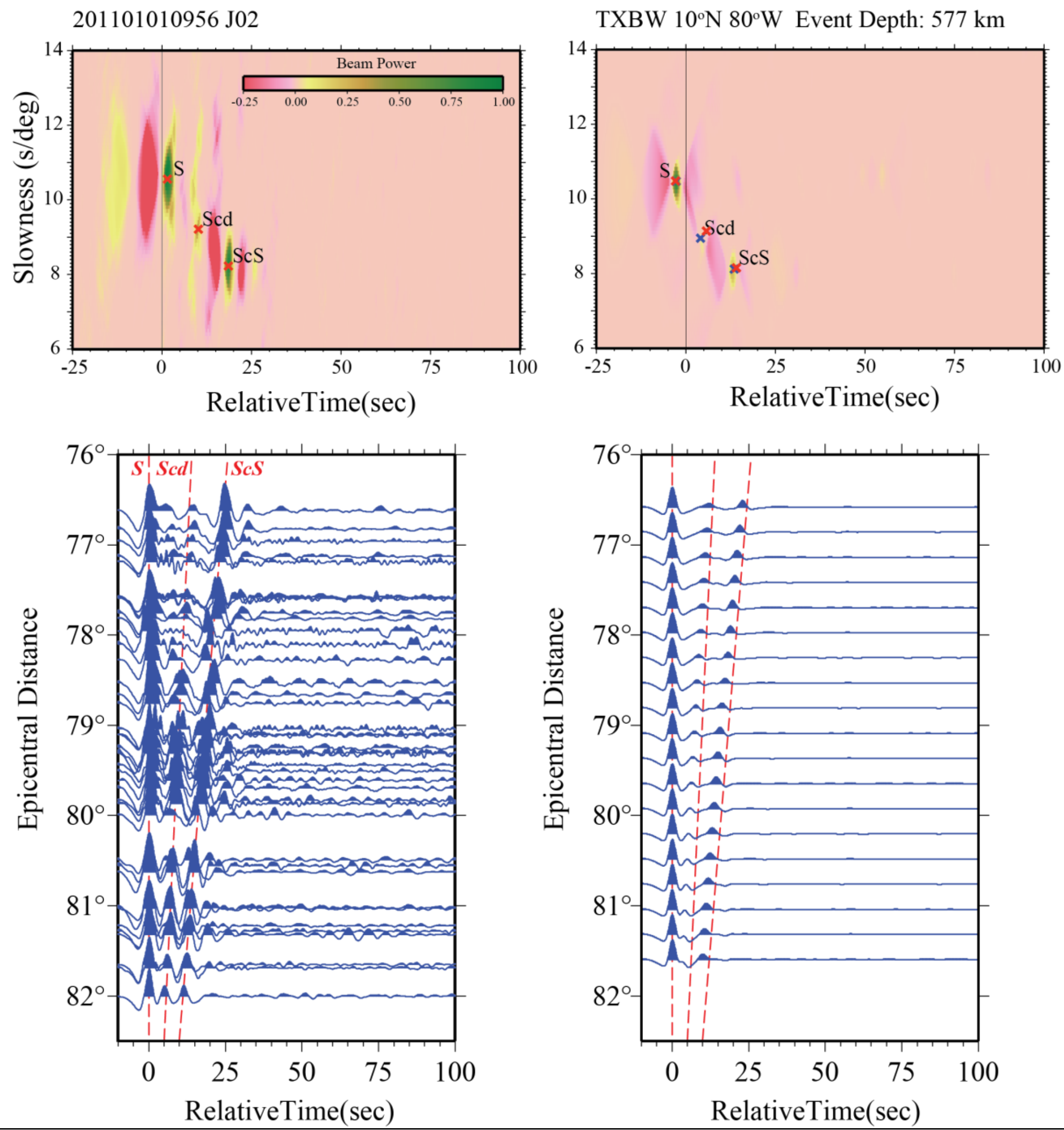

Figure S12. Vespagrams and record sections are shown for data (left hand side) and synthetic seismograms through *S*-wave velocity model TXBW [*Grand*, 2002] (right hand side). Data and synthetics are both for an event depth of 577 km, and sample a central *ScS* bounce point at 10° N, 80° W. The peaks in the vespagrams for data are drawn with red crosses and the peaks in the synthetic vespagrams are drawn with blue crosses. The red crosses for data are repeated in the synthetic vespagram for direct comparison. Note

that absolute time and slowness of data peaks are shifted to be aligned with the direct S-wave arrival in the synthetic vespagram. All traces are displacement transverse component seismograms aligned and normalized to unity on the direct *S*-wave arrival. Approximate arrival times for the *Scd* and *ScS* arrivals for data are indicated by the dashed red lines and repeated in the right-hand column for comparison with synthetic predictions. Synthetic seismograms are shown for a dominant period of 7 s to match the dominant period of data shown in the left-hand column.

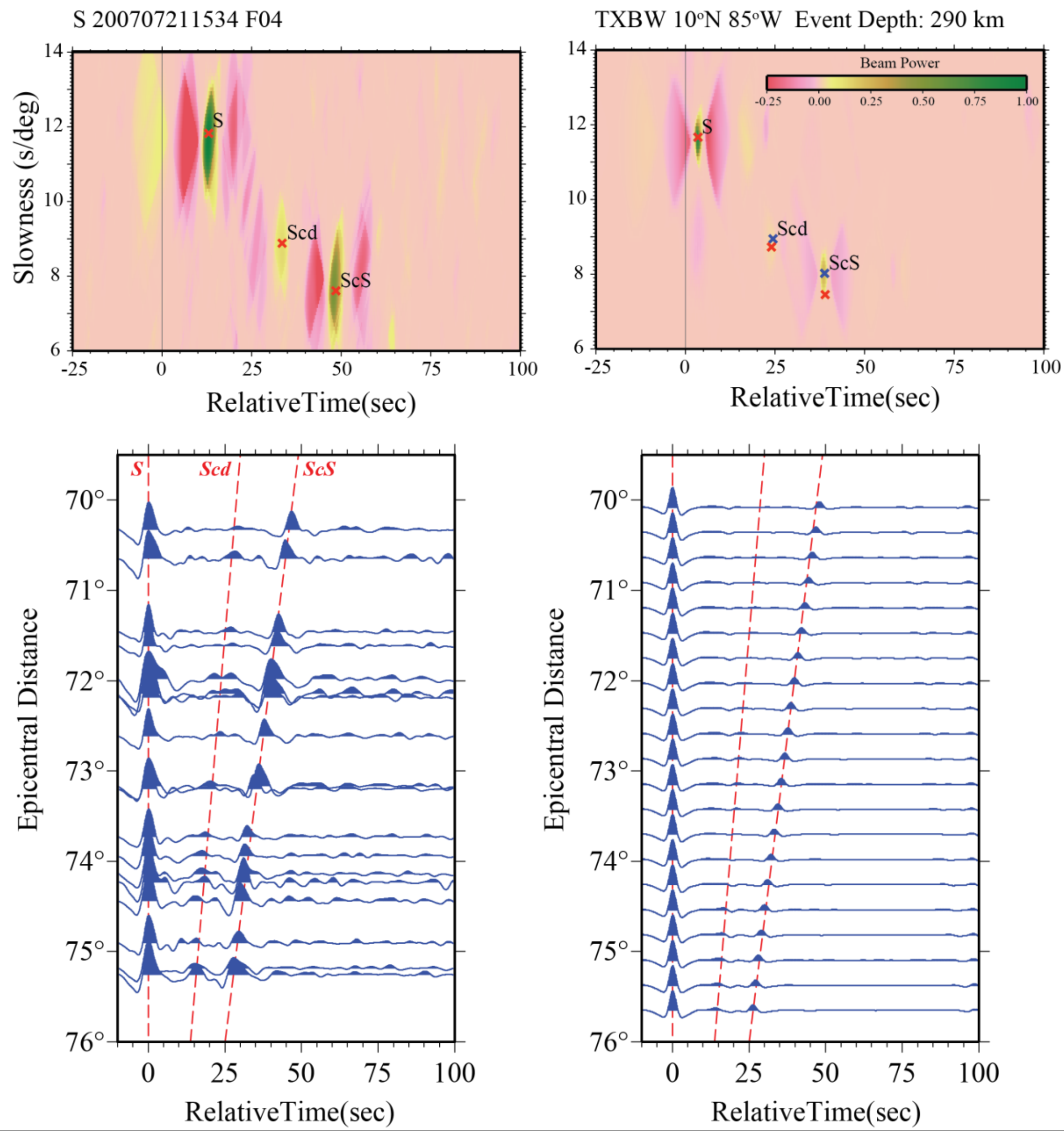

Figure S13. Vespagrams and record sections are shown for data (left hand side) and synthetic seismograms through *S*-wave velocity model TXBW [*Grand*, 2002] (right hand side). Data and synthetics are both for an event depth of 290 km, and sample a central *ScS* bounce point at 10° N, 85° W. The peaks in the vespagrams for data are drawn with red crosses and the peaks in the synthetic vespagrams are drawn with blue crosses. The red crosses for data are repeated in the synthetic vespagram for direct comparison. Note

that absolute time and slowness of data peaks are shifted to be aligned with the direct S-wave arrival in the synthetic vespagram. All traces are displacement transverse component seismograms aligned and normalized to unity on the direct *S*-wave arrival. Approximate arrival times for the *Scd* and *ScS* arrivals for data are indicated by the dashed red lines and repeated in the right-hand column for comparison with synthetic predictions. Synthetic seismograms are shown for a dominant period of 7 s to match the dominant period of data shown in the left-hand column.

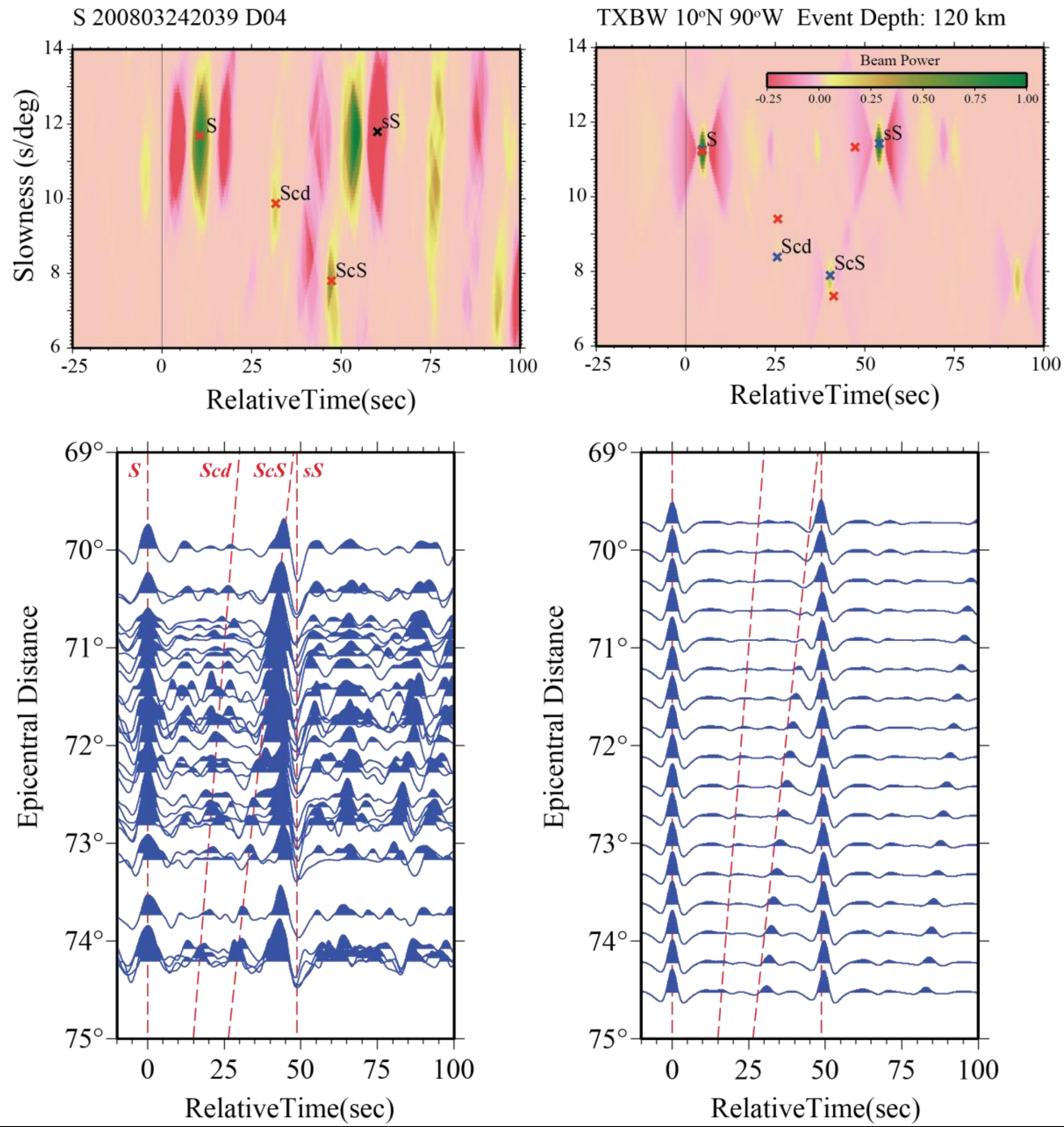

Figure S14. Vespagrams and record sections are shown for data (left hand side) and synthetic seismograms through *S*-wave velocity model TXBW [*Grand*, 2002] (right hand side). Data and synthetics are both for an event depth of 120 km, and sample a central *ScS* bounce point at 10° N, 90° W. The peaks in the vespagrams for data are drawn with red crosses and the peaks in the synthetic vespagrams are drawn with blue crosses. The red crosses for data are repeated in the synthetic vespagram for direct comparison. Note

that absolute time and slowness of data peaks are shifted to be aligned with the direct S-wave arrival in the synthetic vespagram. All traces are displacement transverse component seismograms aligned and normalized to unity on the direct *S*-wave arrival. Approximate arrival times for the *Scd, ScS,* and *sS* arrivals for data are indicated by the dashed red lines and repeated in the right-hand column for comparison with synthetic predictions. Synthetic seismograms are shown for a dominant period of 10 s to match the dominant period of data shown in the left-hand column.

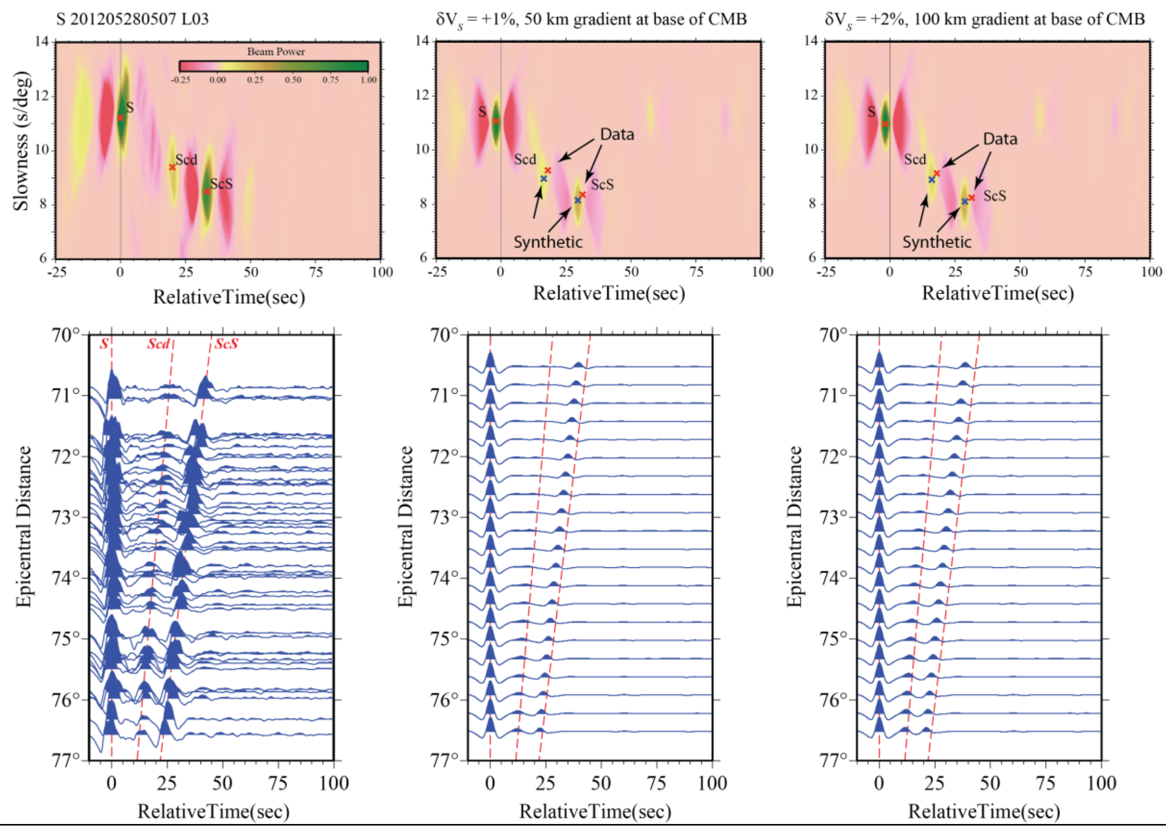

Figure S15. Vespagrams and record sections are shown for data (left hand column) and synthetic seismograms in the middle and right-hand columns. Data and synthetics are both for an event depth of 587 km, and sample a central *ScS* bounce point at 5° N, 75° W. The peaks in the vespagrams for data are drawn with red crosses and the peaks in the synthetic vespagrams are drawn with blue crosses. The red crosses for data are repeated in the synthetic vespagram for direct comparison. Note that absolute time and slowness of data peaks are shifted to be aligned with the direct S-wave arrival in the synthetic vespagram. All traces are displacement transverse component seismograms aligned and normalized to unity on the direct *S*-wave arrival. Approximate arrival times for the *Scd* and *ScS* arrivals for data are indicated by the dashed red lines and repeated in the right-hand column for comparison with synthetic predictions. Synthetic seismograms are

shown for a dominant period of 10 s to match the dominant period of data shown in the left-hand column. Synthetics for the middle column are for a D" discontinuity model as inferred from this study with an *S*-wave velocity jump = +1% and a 50 km thick low velocity gradient zone at the bottom of the mantle. Synthetics for the right-hand column are for a D" discontinuity model as inferred from this study with an *S*-wave velocity jump = +2% and a 100 km thick low velocity gradient zone at the bottom of the mantle.

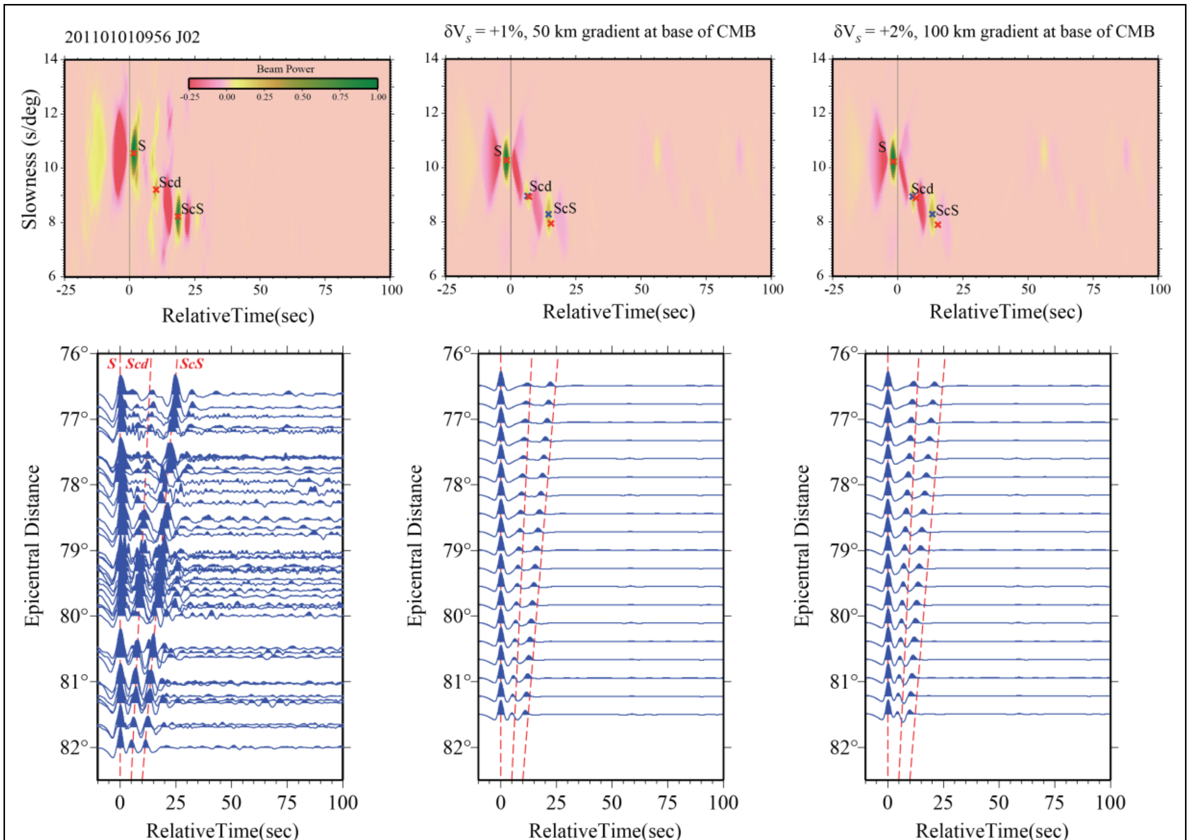

Figure S16. Vespagrams and record sections are shown for data (left hand column) and synthetic seismograms in the middle and right-hand columns. Data and synthetics are both for an event depth of 577 km, and sample a central *ScS* bounce point at 10° N, 80° W. The peaks in the vespagrams for data are drawn with red crosses and the peaks in the synthetic vespagrams are drawn with blue crosses. The red crosses for data are repeated in the synthetic vespagram for direct comparison. Note that absolute time and slowness of data peaks are shifted to be aligned with the direct S-wave arrival in the synthetic vespagram. All traces are displacement transverse component seismograms aligned and normalized to unity on the direct *S*-wave arrival. Approximate arrival times for the *Scd* and *ScS* arrivals for data are indicated by the dashed red lines and repeated in the right-hand column for comparison with synthetic predictions. Synthetic seismograms are

shown for a dominant period of 7 s to match the dominant period of data shown in the left-hand column. Synthetics for the middle column are for a D" discontinuity model as inferred from this study with an *S*-wave velocity jump = +1% and a 50 km thick low velocity gradient zone at the bottom of the mantle. Synthetics for the right-hand column are for a D" discontinuity model as inferred from this study with an *S*-wave velocity jump = +2% and a 100 km thick low velocity gradient zone at the bottom of the mantle.

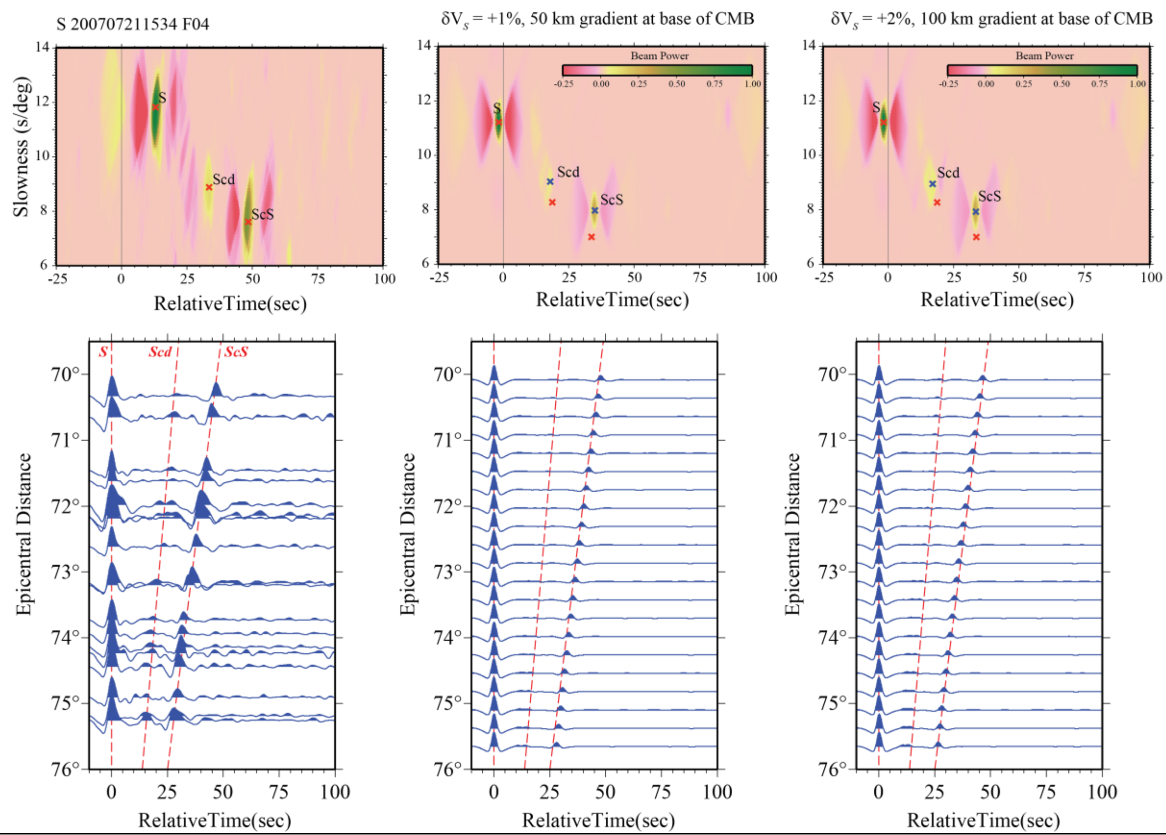

Figure S17. Vespagrams and record sections are shown for data (left hand column) and synthetic seismograms in the middle and right-hand columns. Data and synthetics are both for an event depth of 290 km, and sample a central *ScS* bounce point at 10° N, 85° W. The peaks in the vespagrams for data are drawn with red crosses and the peaks in the synthetic vespagrams are drawn with blue crosses. The red crosses for data are repeated in the synthetic vespagram for direct comparison. Note that absolute time and slowness of data peaks are shifted to be aligned with the direct S-wave arrival in the synthetic vespagram. All traces are displacement transverse component seismograms aligned and normalized to unity on the direct *S*-wave arrival. Approximate arrival times for the *Scd* and *ScS* arrivals for data are indicated by the dashed red lines and repeated in the right-hand column for comparison with synthetic predictions. Synthetic seismograms are

shown for a dominant period of 7 s to match the dominant period of data shown in the left-hand column. Synthetics for the middle column are for a D" discontinuity model as inferred from this study with an *S*-wave velocity jump = +1% and a 50 km thick low velocity gradient zone at the bottom of the mantle. Synthetics for the right-hand column are for a D" discontinuity model as inferred from this study with an *S*-wave velocity jump = +2% and a 100 km thick low velocity gradient zone at the bottom of the mantle.

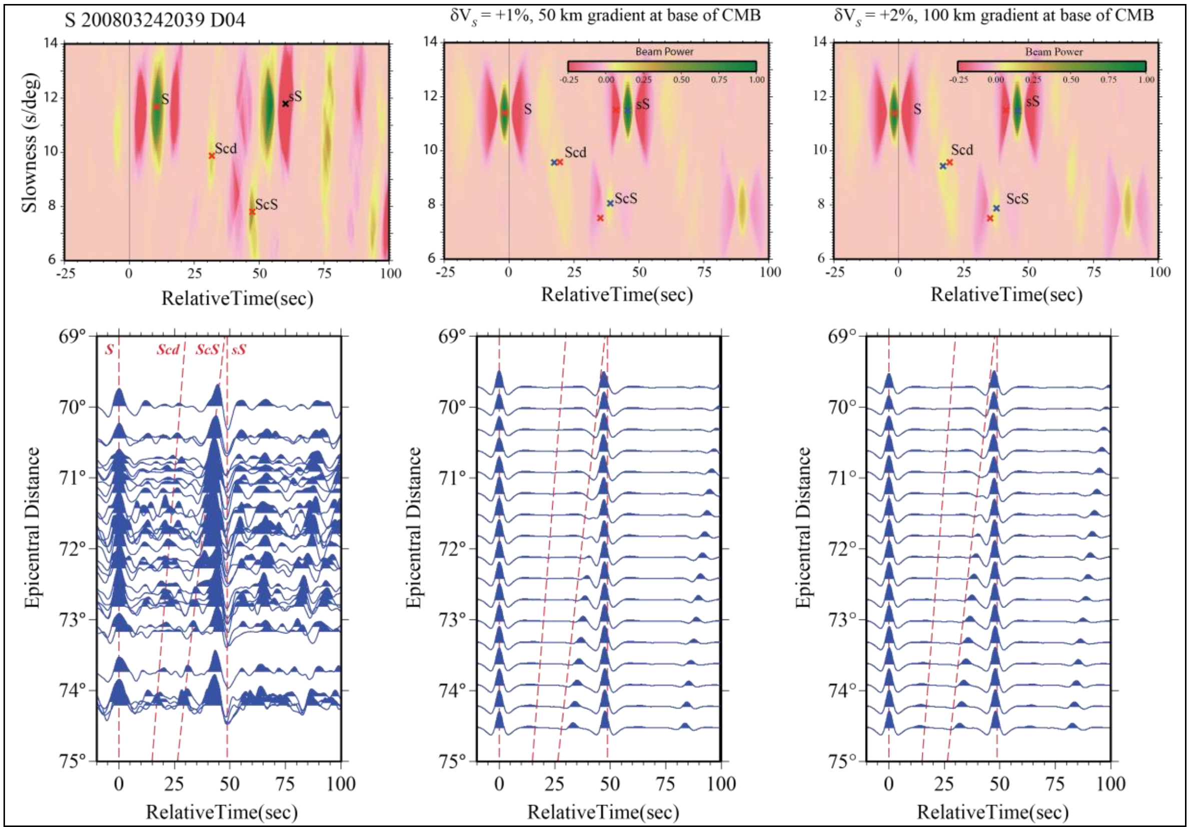

Figure S18. Vespagrams and record sections are shown for data (left hand column) and synthetic seismograms in the middle and right-hand columns. Data and synthetics are both for an event depth of 120 km, and sample a central *ScS* bounce point at 10° N, 90° W. The peaks in the vespagrams for data are drawn with red crosses and the peaks in the synthetic vespagrams are drawn with blue crosses. The red crosses for data are repeated in the synthetic vespagram for direct comparison. Note that absolute time and slowness of data peaks are shifted to be aligned with the direct S-wave arrival in the synthetic vespagram. All traces are displacement transverse component seismograms aligned and normalized to unity on the direct *S*-wave arrival. Approximate arrival times for the *Scd*, *ScS*, and *sS* arrivals for data are indicated by the dashed red lines and repeated in the right-hand column for comparison with synthetic predictions. Synthetic seismograms are shown for a dominant period of 10 s to match the dominant period of data shown in the left-hand column. Synthetics for the middle column are for a D" discontinuity model as inferred from this study with an *S*-wave velocity jump = +1% and a 50 km thick low velocity gradient zone at the bottom of the mantle. Synthetics for the right-hand column are for a D" discontinuity model as inferred from this study with an *S*-wave velocity jump = +2% and a 100 km thick low velocity gradient zone at the bottom of the mantle.

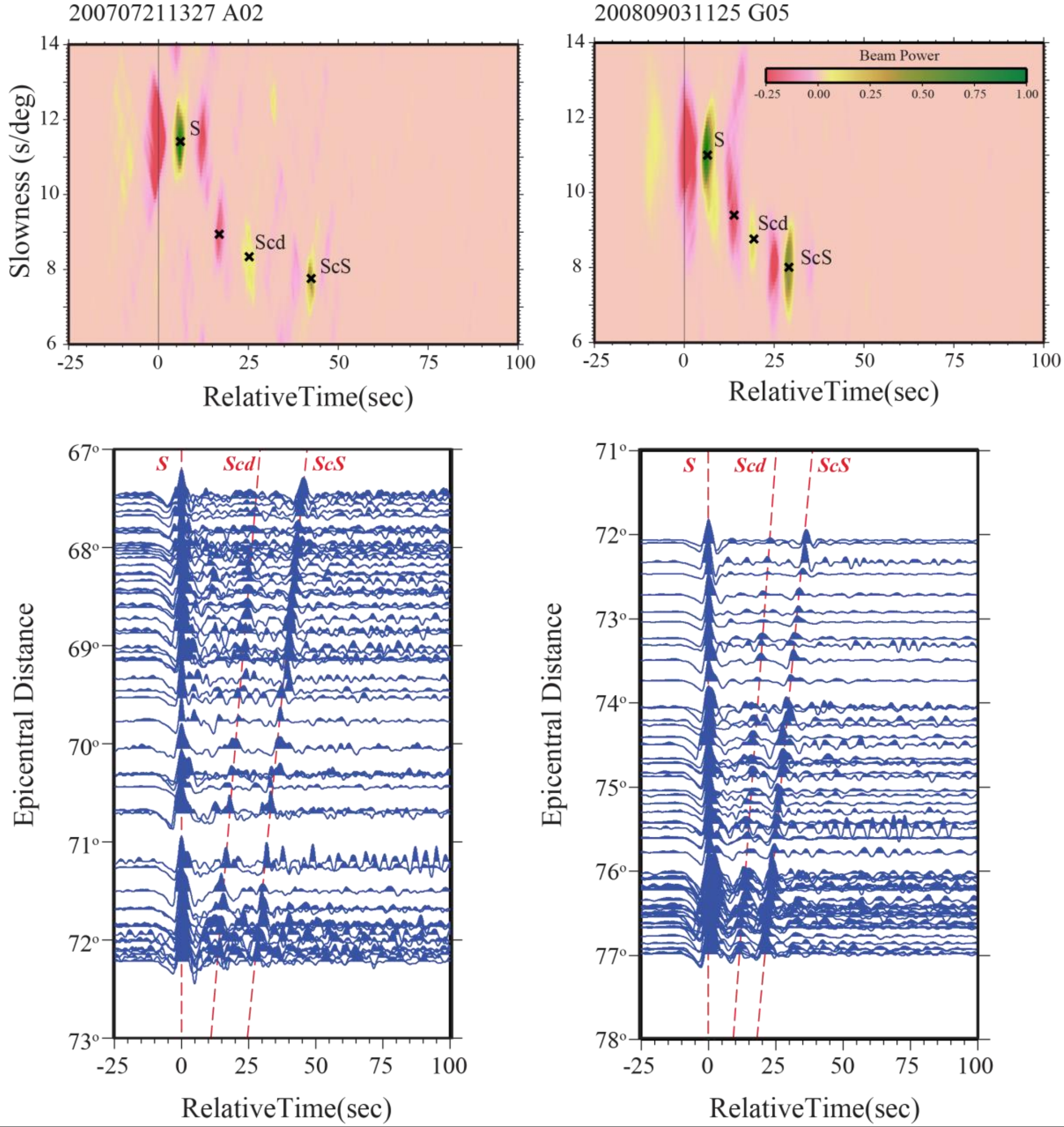

Figure S19. Vespagrams and record sections are shown for two examples that indicate a possible negative impedance reflector above the D" discontinuity. All traces are displacement transverse component seismograms aligned and normalized to unity on the direct *S*-wave arrival. Approximate arrival times for the *Scd* and *ScS* arrivals for data are indicated by the dashed red lines.

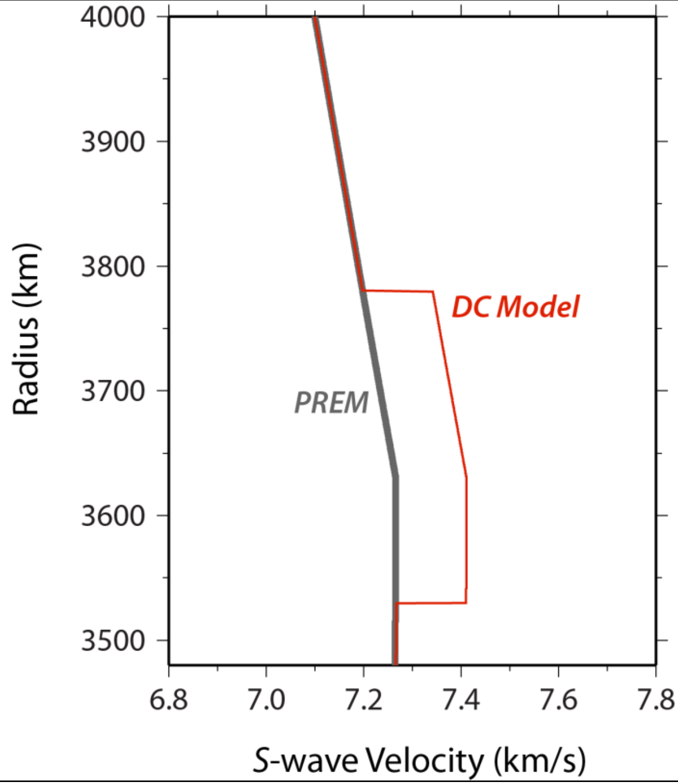

Figure S20. *S*-wave velocity model (orange line) compared to PREM model (gray line) used for double-crossing synthetics shown in Fig. 7b. The model has a D" discontinuity at 300 km above the CMB with a δV_S of 2% and a second discontinuity 50 km above the CMB with a δV_S of 0% with respect to the PREM model.

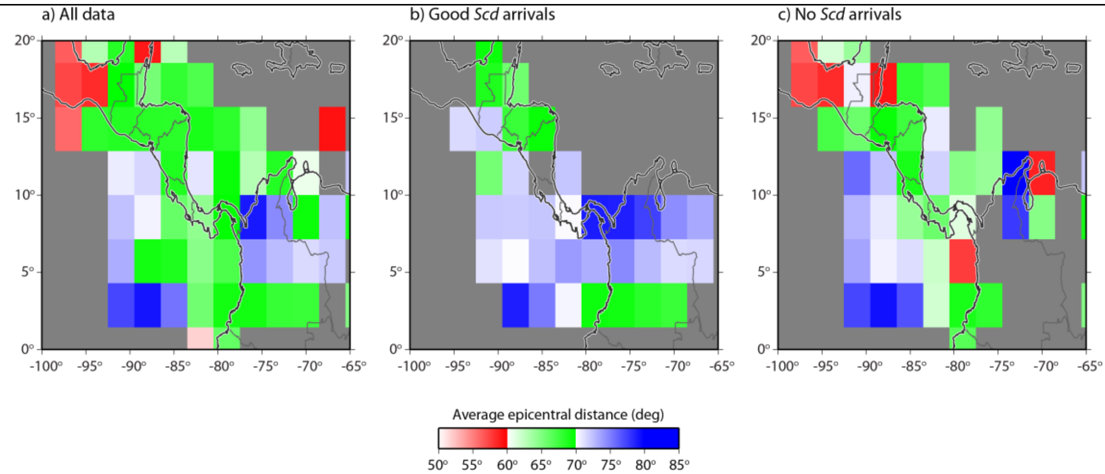

Figure S21. Shown is the average epicentral distance between events and array centroid. The epicentral distances are averaged in 3°×3° geographic bins at the *ScS* bounce point location. Great circle arc distances are shifted to a common event depth of 500 km. (a) Average epicentral distance is shown considering all observations used in this study. (b) Average epicentral distance is shown only considering good *Scd* observations. (c) Average epicentral distance is shown considering all observations that showed no *Scd* arrival.

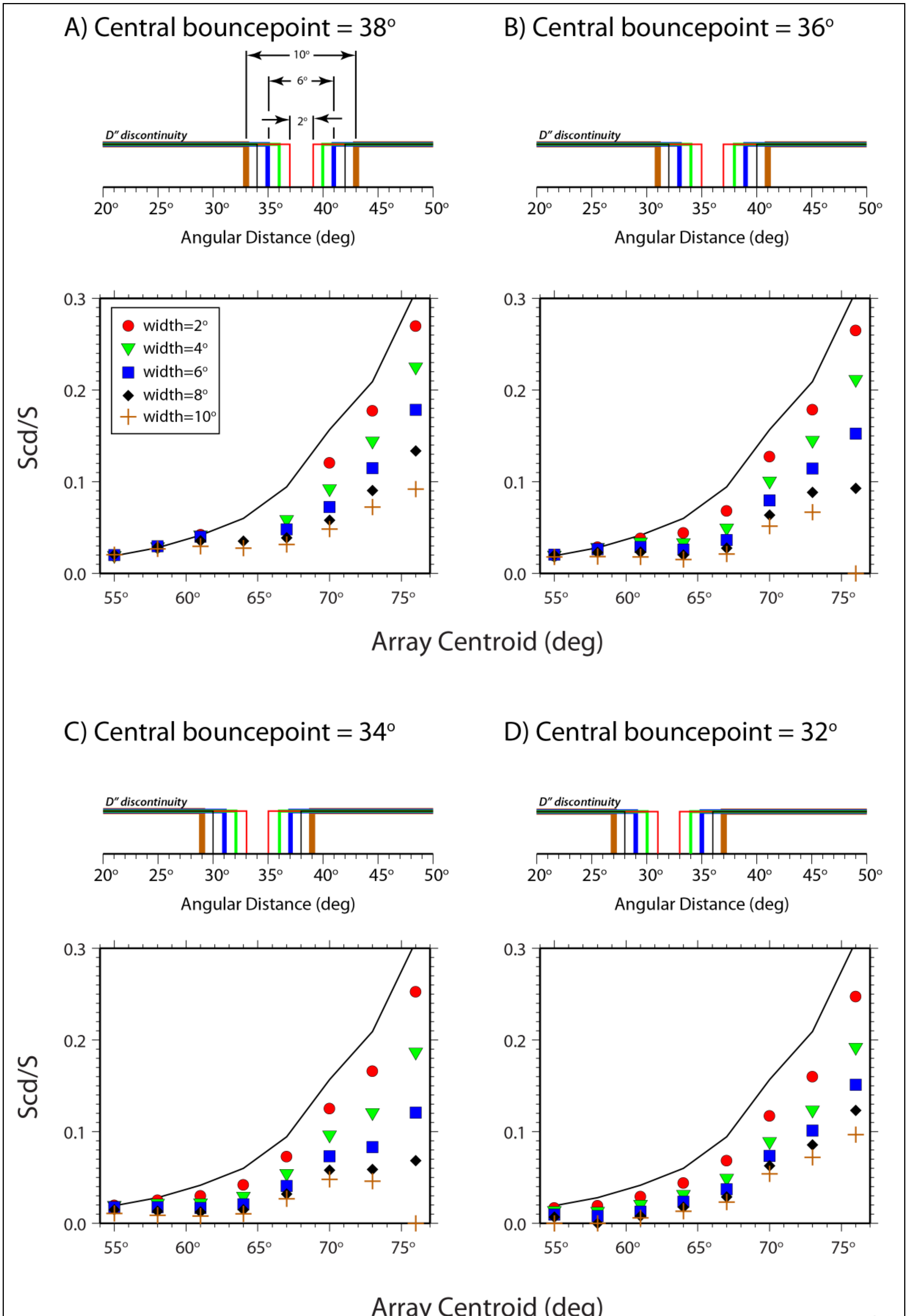
A) Central bouncepoint = 38°
B) Central bouncepoint = 36°
C) Central bouncepoint = 34°
D) Central bouncepoint = 32°
10°
6°
2°
D" discontinuity
Angular Distance (deg)
Scd/S
width=2°
width=4°
width=6°
width=8°
width=10°
Array Centroid (deg)

Figure S22. In each panel the top plot shows a cartoon of the position of the D" discontinuity. It is drawn where the length of the hole in the discontinuity is either 2° (red), 4° (green), 6° (blue), 8° (black), or 10° (orange). The discontinuity *hole* is centered for an *ScS* bounce point on the CMB of a) 38°, b) 36°, c) 34°, and d) 32°. The lower plot of each panel shows the *Scd*/*S* amplitude ratio for each model as a function of the array centroid. In each plot the black line shows the *Scd*/*S* amplitude ratio for a 1-D D" discontinuity model with a height of 300 km and *S*-wave velocity increase of 2%. The colored points correspond to models where the hole has a length of: 2° (red), 4° (green), 6° (blue), 8° (black), or 10° (orange).

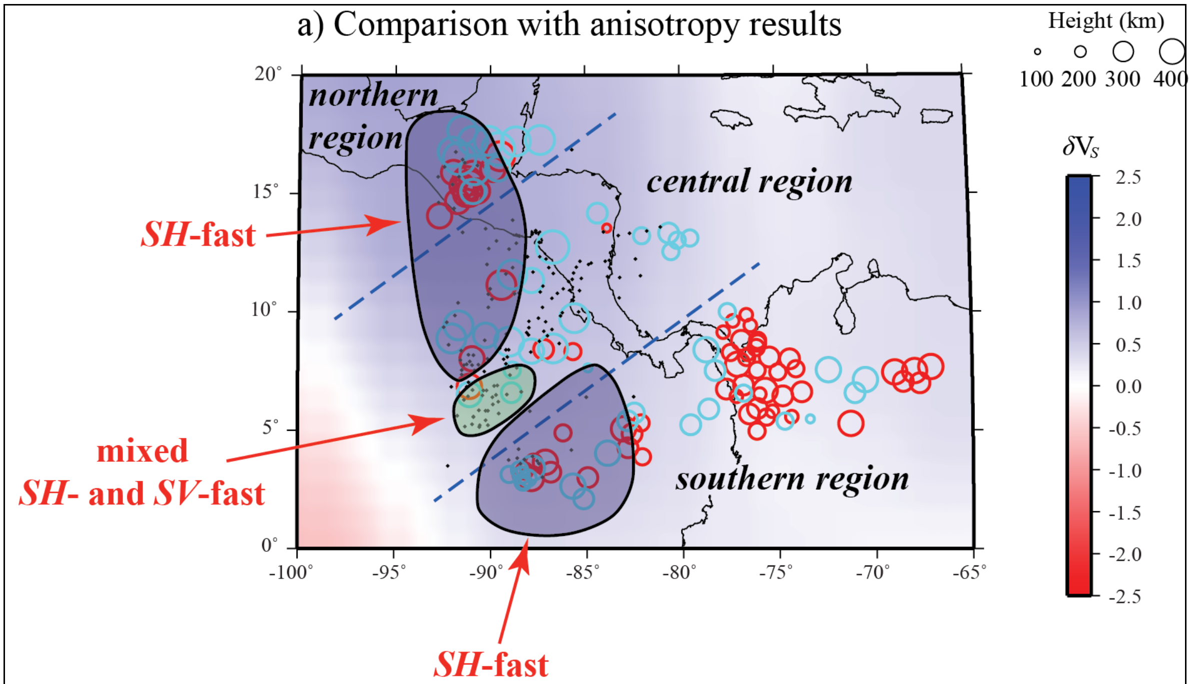

Figure S23. Comparison between our inferred zones (northern, central, and southern regions) with anisotropy results from *Rokosky et al.*, [2004]. The anisotropy results suggest two areas where *SH*- is predominantly fast (areas approximately outlined by purple areas) and one area with a mixture of *SH*- and *SV*-fast (area approximately outlined in green). These areas are overlain with our observations for discontinuity height for the *Scd* observations recorded within the epicentral distance range: $70° \leq \Delta \leq 82°$. The red circles show the locations of *ScS* bounce points for event-array pairs that show strong *Scd* arrivals. The blue circles show possible *Scd* arrivals and the black dots show non-observations. The dashed blue line separates three possible distinct regions of waveform behavior.

Tables

Table 1. Events used in this study

EVENT ID	Latitude	Longitude	Depth (km)	M_w	Records
200506132244	-19.987	-69.197	115.6	6.8	265
200507131206	-17.847	-70.109	79.9	5.9	87
200507261411	-15.345	-72.962	110.5	5.8	73
200508140239	-19.780	-68.980	113.8	5.9	185
200509260155	-5.978	-76.398	115.0	6.7	177
200511171926	-22.319	-67.887	162.6	6.0	252
200512232147	-1.386	-77.517	192.9	5.8	54
200608250044	-24.405	-67.028	184.3	5.9	304
200609121330	-28.944	-68.898	114.0	5.8	194
200609170934	-31.745	-67.176	141.8	6.2	145
200609220232	-26.868	-63.149	598.3	6.1	189
200611130126	-26.041	-63.221	551.8	6.3	322
200705251747	-24.222	-67.027	180.5	5.9	285
200707120523	-7.933	-74.379	152.1	5.9	332
200707211327	-8.133	-71.272	644.9	6.2	386
200707211534	-22.151	-65.777	289.5	5.8	498
200709260443	-3.918	-79.208	99.8	6.1	121
200711160313	-2.312	-77.838	122.9	6.3	358
200711180540	-22.643	-66.323	246.4	6.0	248
200711291900	14.973	-61.263	147.5	6.9	327
200802161445	-21.346	-68.385	130.1	6.1	248
200803242039	-20.043	-68.963	120.0	6.2	350
200807080913	-15.986	-71.748	123.0	5.8	517
200808262100	-7.641	-74.377	154.0	6.0	261
200809031125	-26.736	-63.225	569.6	5.9	517
200810122055	-20.123	-64.971	352.7	6.0	561
200907120612	-15.041	-70.445	198.9	6.1	554
200907141838	-21.822	-67.087	175.6	5.4	293
200909050358	-15.121	-70.248	210.2	5.8	499
200911130727	-17.917	-64.095	608.0	5.8	304
200911141944	-22.965	-66.641	220.4	5.8	437
201001252252	-8.498	-74.466	146.7	5.9	56
201001280804	-23.357	-66.712	208.4	5.8	299
201003042239	-22.227	-68.328	114.0	6.3	487

EVENT ID	Latitude	Longitude	Depth (km)	M_w	Records
201004052236	-19.860	-68.842	94.2	5.8	103
201005190415	-5.074	-77.536	140.0	6.0	102
201005232246	-13.928	-74.352	101.4	6.3	155
201005241618	-8.087	-71.558	581.2	6.0	245
201007120011	-22.146	-68.216	115.0	6.1	450
201008121154	-1.266	-77.306	206.7	6.4	70
201009130715	-14.612	-70.777	179.8	5.9	330
201010221931	-20.878	-68.372	132.2	5.8	222
201101010956	-26.803	-63.136	576.8	6.8	426
201103061231	-18.021	-69.362	118.0	6.0	431
201104021059	-19.576	-69.065	84.4	6.0	185
201104170158	-27.596	-63.201	556.7	5.9	190
201106080306	-17.083	-69.518	145.7	5.8	353
201106201636	-21.701	-68.228	128.0	6.0	520
201108150253	-1.814	-76.908	177.2	5.7	46
201108241746	-7.641	-74.525	147.0	6.8	182
201109021347	-28.398	-63.029	578.9	6.4	461
201111221848	-15.364	-65.090	549.9	6.2	464
201205141000	-17.678	-69.591	105.9	6.4	461
201205280507	-28.043	-63.094	586.9	6.0	569

References

Grand, S. P. (2002), Mantle shear-wave tomography and the fate of subducted slabs, *Philosophical Transactions of the Royal Society London A*, *360*, 2475-2491, doi: 10.1098/rsta.2002.1077.

Hutko, A. R., T. Lay, E. J. Garnero, and J. Revenaugh (2006), Seismic detection of folded, subducted lithosphere at the core–mantle boundary, *Nature*, *441*, 333-336, doi: 10.1038/nature04757.

Kendall, J.-M., and P. M. Shearer (1994), Lateral variations in D" thickness from long-period shear wave data, *J. Geophys. Res.*, *99*(B6), 11,575-511,590.

Kendall, J.-M., and C. Nangini (1996), Lateral variations in D" below the Caribbean, *Geophys. Res. Lett.*, *23*(4), 399-402.

Lay, T., E. J. Garnero, and S. A. Russell (2004), Lateral variation of the D" discontinuity beneath the Cocos Plate, *Geophys. Res. Lett.*, *31*(L15612), doi: 10.1029/2004GL020300.

Rokosky, J. M., T. Lay, E. J. Garnero, and S. A. Russell (2004), High-resolution investigation of shear wave anisotropy in D" beneath the Cocos Plate, *Geophys. Res. Lett., 31, L07605,* doi: 10.1029/2003GL018902.

Shang, X., S.-H. Shim, M. V. De Hoop, and R. D. Van der Hilst (2014), Multiple seismic reflectors in Earth's lowermost mantle, *Proc. Nat. Acad. Sci. U.S.A.*, doi: 10.1073/pnas.1312647111.

Thomas, C., E. J. Garnero, and T. Lay (2004), High-resolution imaging of lowermost mantle structure under the Cocos plate, *J. Geophys. Res.*, *109*(B08307), doi: 10.1029/2004JB003013.